Final Draft

of the original manuscript

Tomchuk, O.; Avdeev, M.; DiDeikin, A.; Vul', A.; Kirilenko, D.; Ivankov, O.; Soloviov, D.; Kuklin, A.; Garamus, V.; Kulvelis, Y.; Aksenov, V.; Bulavin, L.:

Revealing the structure of composite nanodiamond–graphene oxide aqueous dispersions by small-angle scattering.

In: Diamond and Related Materials. Vol. 103 (2020) 107670.

First published online by Elsevier: 24.12.2019

https://dx.doi.org/10.1016/j.diamond.2019.107670

Revealing the structure of composite nanodiamond – graphene oxide aqueous dispersions by small-angle scattering

Tomchuk O.V.[1,2,], Avdeev M.V.[1], Dideikin A.T.[3], Vul' A.Ya.[3], Aleksenskii A.E.[3], Kirilenko D.A.[3], Ivankov O.I.[1,4,5], Soloviov D.V.[1,4,5], Kuklin A.I.[1,5], Garamus V.M.[6], Kulvelis Yu.V.[7], Aksenov V.L[7,1], Bulavin L.A.[2,4]*

[1] Frank Laboratory of Neutron Physics, Joint Institute for Nuclear Research, Dubna 141980, Russia

[2] Faculty of Physics, Taras Shevchenko National University of Kyiv, Kyiv 03022, Ukraine

[3] Ioffe Institute, St.Petersburg 194021, Russia

[4] Institute for Safety Problems of Nuclear Power Plants, Chornobyl 07270, Ukraine

[5] Moscow Institute of Physics and Technology, Dolgoprudny 141701, Russia

[6] Helmholtz-Zentrum Geesthacht, Centre for Materials and Coastal Research, Geesthacht 21502, Germany

[7] National Research Centre "Kurchatov Institute", 123182 , Moscow, Russia

* *Corresponding author: tomchuk@jinr.ru*

Abstract

The work presents the results of studying the structure of binary liquid nanocarbon systems obtained by mixing hydrosol of detonation nanodiamond and aqueous dispersions of single layer graphene oxide flakes. We studied size and space distribution of nanocarbon clusters formed upon interaction of the components in aqueous media by mutually complement methods of small-angle X-ray and neutron scattering. The formation of small secondary agglomerates of nanodiamond particles on the surface of graphene oxide flakes was concluded and supported by the data of transmission electron microscopy from dried samples. The observed effect can significantly modify the structure of nanocarbon composites formed of nanodiamond and graphene oxide. The structural features of binary dispersions detonation nanodiamond–graphene oxide should be taken into account at the preparation of the conductive composites of carbon nanoonions and reduced graphene oxide for energy storage systems.

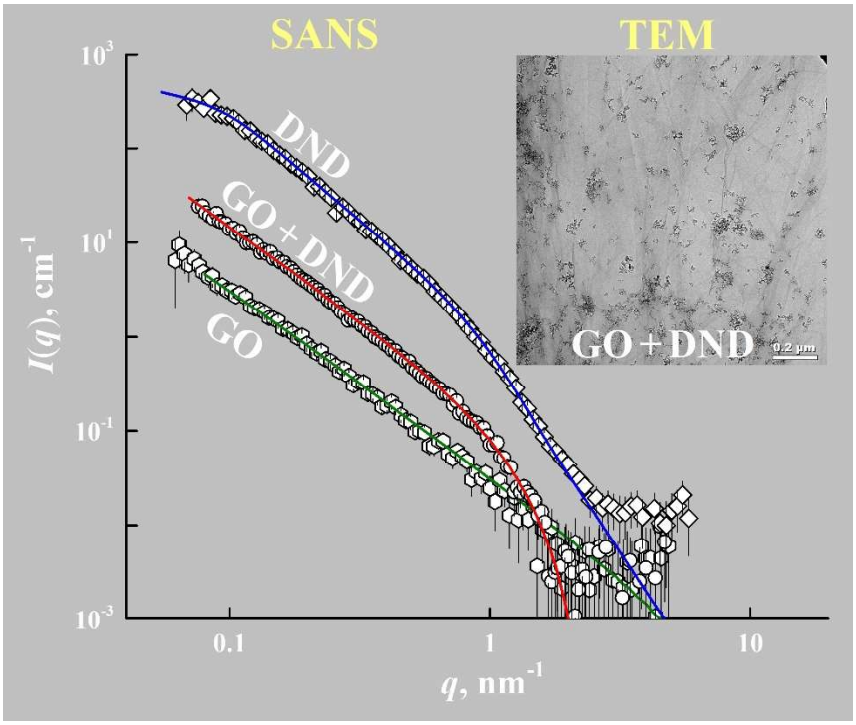
SANS
TEM
DND
GO + DND
GO
GO + DND
0.2 μm
10^3
10^1
10^{-1}
10^{-3}
$I(q)$, cm^{-1}
0.1
1
10
q, nm^{-1}

Introduction

Graphene (a single layer of graphite in which sp2-bonded carbon atoms form a two-dimensional hexagonal lattice) due to its unique electronic [1,2,6], as well as mechanical [3, 5] and thermal [4] properties is an extremely popular material with widest range of promising applications. The synthesis of large area graphene conductive coatings for solar cells and high specific area electrodes for supercapacitors and rechargeable batteries often starts with aqueous suspensions of graphene oxide (GO) [7,8] as intermediate state. As compared to pure graphene, the suspensions of GO are stable due to the high negative surface charge formed because of hydroxyl groups attached to the graphene plain [9]. A problem in application of these suspensions is uncontrollable formation of folds and wrinkles in resulting graphene sheets due to vanishing of the surface charge while removing the water before reduction of GO to graphene. In consequence, local topography strongly affects π-bonds varying the reactivity of the graphene [10]. The density and mobility of the charge carriers in wrinkled graphene show drastic difference with respect to the ideally flat graphene sheet [11,12].

Using nanoparticles has recently become an appropriate tool for controlling graphene topography at nanoscale [13]. The widely known detonation nanodiamonds (DND) [14,15] are one of the main candidates for such applications. Applying the composite material of graphene oxide and particles of detonation nanodiamond with appropriate combination of surface potentials could be the complete solution of the problem opening the wide range of new application areas of graphene-based materials. The preliminary results of TEM study have shown the noticeable removal of folds and wrinkles of graphene sheets due to presence of separate DND particles.

Preparation of binary aqueous dispersions of diamond nanoparticles and single layer graphene oxide flakes is a key step in the synthesis of a new type of carbon nanocomposites with tunable set of parameters including conductance, specific surface area, porosity and sorption capacity. A Subsequent simultaneous thermal transformation of graphene oxide to graphene and nanodiamonds to carbon onions opens prospective for application of the composite in new generation of energy storage devices like ultra-capacitors and lithium batteries, catalytic systems, photo catalysts, tunable sorbents and membranes for environmental protection technologies [16-20].

The main problem in studying the structure of clusters of nanoparticles in liquid dispersions by high resolution direct space methods such as electron (TEM, SEM) or atomic force (AFM) microscopy is the necessity to remove in the experiment the liquid phase, which can cause significant structural changes and distortions in the system under study. Widespread dynamic

light scattering (DLS) dealing with liquid dispersions and sols has restrictions due to its reconstructive basis with respect to solutions with developed aggregation. In this connection, scattering methods such as small-angle X-ray (SAXS) and neutron (SANS) scattering are most suitable for structural studies of clusterized liquid dispersions. Here, these methods were applied to liquid dispersions of carbon nanostructures including detonation nanodiamonds, graphene oxide and their combinations. The previous studies of DND particles in hydrosols with various types of stabilization [15, 21-26] demonstrated well the applicability of SAXS and SANS to characterize particles and their clusters in a wide concentration range including the conditions of the sol-gel transition. Together with the particle size distribution parameters, a fine particle structure was revealed showing a clear density gradient at the surface of the particles. The main feature of the clusters observed is that there is a universal aggregation mechanism in such systems resulting in a common scaling of the clusters presumably due to a specific charge distribution on DND particle surface.

Thus, it is worth considering small-angle scattering methods as an effective approach for revealing the initial stages of the DND/GO composite formation because of interaction of the components of binary (DND particles and GO flakes) aqueous dispersions. The main goal of the current study was to understand the structuring process of single-layer graphene oxide flakes with particles of detonation nanodiamond in the mixed aqueous dispersions at the initial stage of the preparation of diamond–graphene nanocomposite by scattering techniques including SAXS and SANS. The structure is analyzed by comparing the specific features of the mixed solutions with the details of GO sheets and DND clusters in the partial aqueous dispersions. The results are compared with the DLS data and TEM from dried samples.

Materials and methods

We prepared GO from natural crystalline graphite by modified Hammers process, the same as in work [28]. Avoiding usage of ultrasonic at oxidation stage allowed obtaining mean size of single layer GO flakes as 30 μm. Fig. 1a demonstrates size distribution of GO flakes obtained applying light diffraction using Mastersizer 2000 (by Malvern Instruments). Keeping large size of GO flakes allowed reducing contribution of edge states of GO sheets to interaction with DND. The initial concentration of GO flakes in prepared aqueous dispersion amounted 0.5 wt. %.

For preparation the samples DND dry powders provided by FSUE ‘Technolog’, (St Petersburg, Russia) were used. Procedure of additional purifying the material and subsequent deagglomeration corresponds in details to the method described in [27]. For thermal stage of the

process we used annealing in hydrogen and obtained stable hydrosol of DND. Zeta-potential of particles in hydrosol was 50 mV. Maximum of size distribution of diamond nanoparticles (Fig. 1b) comprised 4.5 nm. Actual range of particle sizes, determined by DLS using Zetasizer Nano ZS (Malvern Instruments) was from 3 to 10 nm. The initial concentration of prepared DND hydrosol was 0.7 wt. %.

The required increase of concentration of dispersion was performed by centrifugation of initial dispersion. We also applied partial removal of water from dispersion using vacuum evaporator. For preparation of binary aqueous dispersions of DND and GO aqueous dispersions were diluted/concentrated for required concentrations and subsequently mixed in corresponding ratios using mechanical mixer.

Samples for the TEM study were prepared by drop-casting of binary aqueous dispersions on copper supporting meshes for electron microscopy. Samples were dried in vacuum at room temperature and subsequently heated up to 320°C for complete removal of water. TEM images of DND–GO composite were obtained using Jeol JEM-2100F instrument, (200 kV, point-to-point resolution of 0.19 nm).

The SANS study has been carried out on the YuMO time-of-flight two-detector small-angle diffractometer at the 4th channel of IBR-2 pulsed neutron source (Joint Institute for Nuclear Research, Dubna, Russia) [29]. Neutron wavelengths within a range of 0.05–0.5 nm and sample–detector distances of 4.5 and 13 m were used to obtain scattering curves in a q-range of 0.7–5 nm^{-1}. A vanadium standard was used for an absolute calibration of the differential cross-section. The raw data treatment was performed by the SAS program with a smoothing mode [30]. All SANS measurements were made in Hellma plane quartz cells (path length 1 mm), while in the SAXS experiments, the samples were placed into 1 mm diameter glass capillaries with a diameter of 1 mm. The complementary SAXS experiments were performed at the P12 BioSAXS Beamline (EMBL/DESY) at PETRA III ring of the DESY synchrotron (Hamburg, Germany) [31]. The scattering curves calibrated with respect to the transmitted beam intensity were obtained in the q-range of 0.04–5 nm^{-1} using a Pilatus 2 M pixel detector placed at the sample-to-detector distance of 3.1 m and X-ray radiation wavelength of 0.124 nm.

Results and discussion

The experimental curves of small-angle scattering on GO aqueous suspensions obtained for one system at different times at different facilities are shown in Fig. 2a. They indicate that scattering occurs on a two-dimensional structure, since the power law of scattering is described by the

exponent –2. This is a strong argument in favor of the fact that oxidized graphene on a scale of 1–100 nm really has a flat shape and looks more like a flat sheet of paper, rather than wrinkled. A different form-factor, or at least an exponent other than two, would hypothetically characterize the latter case. Judging by the multitude of published data and general considerations, small-angle scattering by graphene oxide can be approximated using the cylinder form factor [32]. The shape of graphene flakes in the form of thin disks suggests the presence of two distinguished sizes – diameter and thickness. The Guinier mode, which describes the diameter, is not observed in the initial part of the curve (low q), due to the resolution restriction of the conventional SAXS/SANS instruments with respect to micron sizes (detected sizes $< 2\pi/q_{min}$). This completely correlates with the light scattering data (Fig. 1a) presented above, indicating a diameter of flakes of tens of micrometers. On the contrary, at the end of the curve there is a kink, which is responsible for the thickness. Despite the high residual incoherent background, the thickness of graphene flakes can be estimated from the fitting at the level of 0.5(1) nm, which completely corresponds to a single graphene layer. Thus, SAXS/SANS data show, first, the two-dimensional structure of GO, and, second, the fact that they consist of a single layer of graphene, thus confirming the high efficiency of the synthesis method [28] for producing GO mostly in the form of single-layer flakes.

To investigate the influence of DND particles on the structure of oxidized graphene, first, aqueous dispersions of nanodiamonds were studied by SANS. Similar to the previous experiment with such materials [15,24–26], SANS curves demonstrated a two-level organization combining scattering from a diffuse surface of diamond particles collected in fractal clusters with a fractal dimension, $D \sim 2.3$, which is equal in magnitude to the power-law scattering exponent (Fig. 1b). The inset in Fig. 1b shows that the scattering curves normalized to the weight fraction of nanodiamonds in the system repeat each other except for the initial part (small q), where the influence of the structural factor (i.e., cluster-cluster interaction) is stronger for more concentrated systems; and also the end part, where the influence of the residual incoherent background produced by hydrogen atoms is manifested. An important aspect is that an aqueous DND suspension always contains both clusters of different sizes and non-aggregated nanoparticles in comparable amounts [15,34].

In the frame of the study, several aqueous suspensions of graphene oxide and detonation nanodiamonds were prepared, which were then mixed in different proportions, which in practice is most conveniently described by the mass ratio of the two components of the dispersion:

$$\chi = m_{GO}/m_{DND} \qquad (1)$$

The initial SANS curves for GO+DND system, as well as normalized to the DND concentration, for the mixtures with different χ-parameter are shown in Fig. 1c. The effect of a suspension structuring is clearly observed at high graphene loadings. While there is little graphene in the system, SANS can distinguish only nanodiamonds, since the curves are similar to those for cluster suspensions of DNDs (Fig. 2b). Similarly, normalized curves repeat each other and can be described by a model of fractal clusters [33] with a fractal dimension of 2.3. However, when the amount of graphene in the system overcomes some critical value, and it becomes quite a lot (in our case, 2.4 times more by mass than nanodiamond), the scattering pattern changes significantly. The dimension of the objects decreases to 2. That is, we again deal mainly with flat scatterers, as in the case of pure oxide without DND additives. Nevertheless, the kink at large q, which is responsible for the flake transverse size, is much to the left, indicating a thickening of the graphene sheet. In this case, approximation by a model of a thin disk gives 2.7(2) nm.

Two hypotheses were put forward to explain this observation. The first one assumes the adhesion of individual graphene flakes under the action of DND particles, which could be observed as a thickening of the scatterer from the SANS point of view. The second hypothesis explains the effective thickening by binding of DND particles and, possibly, clusters with individual GO flakes. An electron microscopy experiment confirmed the second hypothesis. A typical TEM image is shown in Fig. 3. It shows binding of clusters of various sizes, down to the smallest, including separate diamond nanocrystallites, with a GO monolayer.

Thus, using small-angle scattering and complementary techniques, we were able to study both the initial components and the final aqueous suspension of GO+DND, and to detect the effect of the binding of DND particles and clusters to monolayers of graphene oxide in an aqueous medium. Fig. 4 schematically shows the structure of the obtained GO+DND composite, as well as how two methods, microscopy (direct space) and small-angle diffraction (reciprocal space), could detect the structural aspects of thin layers of graphene oxide nanosystems. The main difference is that TEM is a local method, and small-angle scattering receives averaged information about all dispersed particles. This property should be widely used in various studies of nanosystems, since these two techniques perfectly complement each other.

In addition to the mass ratio effect, the final structure of the composite material can be affected by the preparation procedure, in particular, the mixing regime. To exclude the effect of mixing conditions on the results of the study, we prepared mixtures of GO and DND aqueous suspensions by relatively slight (< 60 rpm) and intensive (> 300 rpm) mixing. The results presented in Fig. 5 indicate that the formation of the composite material does not depend on the

mixing mode, but is determined solely by the physicochemical characteristics of the surface of the studied carbon nanoparticles.

Conclusions

Our data strongly confirm the two-dimensional structure organization of the graphene oxide sheets, as well as the fact that they consist of a single graphene-type layer. Despite the existence of large brunched clusters in the concentrated liquid dispersions of nanodiamonds combined also in the aggregates, these systems are structurally stable. With respect to the composite, the binding of individual nanodiamond particles as well as their small fractal clusters together with their homogeneous and random distribution along the graphene planes has been concluded basing on the analysis of the scattering data.

Acknowledgements

The financial support of the Russian Foundation for Basic Research (project No. 18-29-19159) is acknowledged. The authors gratefully acknowledge Clement Blanchet for the help during the X-ray scattering experiments at the P12 BioSAXS beamline (EMBL/DESY, PETRA III).

Refferences

[1] K.S. Novoselov, A.K. Geim, S.V. Morozov, D. Jiang, Y. Zhang, S.V. Dubonos, I.V. Grigorieva, A.A. Firsov, Electric field effect in atomically thin carbon films, Science 306 (2004) 666-669, https://doi.org/10.1126/science.1102896

[2] K.S. Novoselov, A.K. Geim, S.V. Morozov, D. Jiang, M.I. Katsnelson, I.V. Grigorieva, S.V. Dubonos, A.A. Firsov, Two-dimensional gas of massless Dirac fermions in graphene, Nature 438 (2005) 197-200, https://doi.org/10.1038/nature04233

[3] T.J. Booth, P. Blake, R.R. Nair, D. Jiang, E.W. Hill, U. Bangert, A. Bleloch, M. Gass, K.S. Novoselov, M.I. Katsnelson, A.K. Geim, Macroscopic graphene membranes and their extraordinary stiffness, Nano Lett. 8 (2008) 2442-2446, https://doi.org/10.1021/nl801412y

[4] A.A. Balandin, S. Ghosh, W. Bao, I. Calizo, D. Teweldebrhan, F. Miao, C.N. Lau, Superior thermal conductivity of single-layer graphene, Nano Lett. 8 (2008) 902-907, https://doi.org/10.1021/nl0731872

[5] J.S.Bunch, S.S. Verbridge, J.S. Alden, A.M. van der Zande, J.M. Parpia, H.G. Craighead, P.L. McEuen, Impermeable atomic membranes from graphene sheets, Nano Lett. 8 (2008) 2458-2462, https://doi.org/10.1021/nl801457b

[6] S.V. Morozov, K.S. Novoselov, M.I. Katsnelson, F. Schedin, D.C. Elias, J.A. Jaszczak, A.K. Geim, Giant intrinsic carrier mobilities in graphene and its bilayer, Phys. Rev. Lett. 100 (2008) 016602, https://doi.org/10.1103/PhysRevLett.100.016602

[7] P. Pasanen, M. Voutilainen, M. Helle, X. Song, P.J. Hakonen, Graphene for future electronics, Phys. Scr. T146 (2012) 014025, https://doi.org/10.1088/0031-8949/2012/T146/014025

[8] X. Huang, Z. Yin, S. Wu, X. Qi, Q. He, Q. Zhang, Q. Yan, F. Boey, H. Zhang, Graphene-based materials: synthesis, characterization, properties, and applications, Small 7 (14) (2011) 1876-1902, https://doi.org/10.1002/smll.201002009

[9] K.P. Loh, Q. Bao, G. Eda, M. Chhowalla, Graphene oxide as a chemically tunable platform for optical applications, Nat. Chem. 2 (2010) 1015-1024, https://doi.org/10.1038/nchem.907

[10] M.A. Bissett, S. Konabe, S. Okada, M. Tsuji, H. Ago, Enhanced chemical reactivity of graphene induced by mechanical strain, ACS Nano 7 (2013) 10335–10343, https://doi.org/10.1021/nn404746h

[11] T. Low, F. Guinea, Strain-induced pseudomagnetic field for novel graphene electronics, Nano Lett. 10 (2010) 3551–3554, https://doi.org/10.1021/nl1018063

[12] V.M. Pereira, A.H. Castro Neto, Strain engineering of graphene's electronic structure, Phys. Rev. Lett. 103 (2009) 046801, https://doi.org/10.1103/PhysRevLett.103.046801

[13] J. Vejpravova, B. Pacakova, J. Endres, A. Mantlikova, T. Verhagen, V. Vales, O. Frank, M. Kalbac, Graphene wrinkling induced by monodisperse nanoparticles: facile control and quantification, Sci. Rep. 5 (2015) 15061, https://doi.org/10.1038/srep15061

[14] E. Ōsawa, Monodisperse single nanodiamond particulates, Pure Appl. Chem. 80 (7) (2008) 1365-1379, https://doi.org/10.1351/pac200880071365

[15] O.V. Tomchuk, M.V. Avdeev, A.E. Aleksenskii, A.Ya. Vul, O.I. Ivankov, V.V. Ryukhtin, J. Füzi, V.M. Garamus, L.A. Bulavin, Sol-gel transition in nanodiamond aqueous dispersions by small-angle scattering, J. Phys. Chem. C 123 (29) (2019) 18028-18036, https://doi.org/10.1021/acs.jpcc.9b03175

[16] S.J. Rowley-Neale, E.P. Randviir, A.S. Abo Dena, C.E. Banks, An overview of recent applications of reduced graphene oxide as a basis of electroanalytical sensing platforms, Appl. Mater. Today 10 (2018) 218-226, https://doi.org/10.1016/j.apmt.2017.11.010

[17] H. Ahmad, M. Fan, D. Hui, Graphene oxide incorporated functional materials: A review, Compos. Part B Eng. 145 (2018) 270-280, https://doi.org/10.1016/j.compositesb.2018.02.006

[18] A.T. Dideikin, A.Y. Vul'. Graphene oxide and derivatives: The place in graphene family, Front. Phys. 6. (2019) 149, https://doi.org/10.3389/fphy.2018.00149

[19] D. Chen, H. Feng, J. Li, Graphene oxide: Preparation, functionalization, and electrochemical applications, Chem. Rev. 112 (2012) 6027-6053, https://doi.org/10.1021/cr300115g

[20] A. Bianco, Y. Chen, Y. Chen, D. Ghoshal, R.H. Hurt, Y.A. Kim, N. Koratkar, V. Meunier, M. Terrones, A carbon science perspective in 2018: Current achievements and future challenges, Carbon 132 (2018) 785-801, https://doi.org/10.1016/j.carbon.2018.02.058

[21] M.V. Avdeev, V.L. Aksenov, O.V. Tomchuk, L.A. Bulavin, V.M. Garamus, E. O□sawa, The spatial diamond-graphite transition in detonation nanodiamond as revealed by small-angle neutron scattering, J. Phys.: Condens. Matter 25 (2013) 445001, https://doi.org/10.1088/0953-8984/25/44/445001

[22] O.V. Tomchuk, L.A. Bulavin, V.L. Aksenov, V.M. Garamus, O.I. Ivankov, A.Ya. Vul', A.T. Dideikin, M.V. Avdeev, Small-angle scattering from polydisperse particles with a diffusive surface, J. Appl. Cryst. 47 (2014) 642-653, https://doi.org/10.1107/S1600576714001216

[23] N.M. Kuznetsov, S.I. Belousov, D.Yu. Stolyarova, A.V. Bakirov, S.N. Chvalun, A.V. Shvidchenko, E.D. Eidelmand, A.Ya. Vul', Effect of diamond nanoparticle chains on rheological properties of hydrosol, Diam. Relat. Mater. 83 (2018) 141-145, https://doi.org/10.1016/j.diamond.2018.02.006.

[24] M.V. Avdeev, N.N. Rozhkova, V.L. Aksenov, V.M. Garamus, R. Willumeit, E. O□sawa, Aggregate structure in concentrated liquid dispersions of ultrananocrystalline diamond by small-angle neutron scattering, J. Phys. Chem. C 113 (22) (2009) 9473-9479, https://doi.org/10.1021/jp900424p

[25] O.V. Tomchuk, M.V. Avdeev, V.L. Aksenov, V.M. Garamus, L.A. Bulavin, S.N. Ivashevskaya, N.N. Rozhkova, N. Schreiber, J. Schreiber, Comparative structural characterization of the water dispersions of detonation nanodiamonds by small-angle neutron scattering, J. Surf. Invest. 6 (2012) 821-824, https://doi.org/10.1134/S1027451012100151

[26] M.V. Avdeev, O.V. Tomchuk, O.I. Ivankov, A.E. Alexenskii, A.T. Dideikin, A.Ya. Vul, On the structure of concentrated detonation nanodiamond hydrosols with a positive potential: Analysis of small-angle neutron scattering, Chem. Phys. Lett. 658 (2016) 58-62, https://doi.org/10.1016/j.cplett.2016.06.010

[27] A.T. Dideikin, A.E. Aleksenskii, M.V. Baidakova, P.N. Brunkov, M. Brzhezinskaya, V.Yu. Davydov, V.S. Levitskii, S.V. Kidalov, Yu.A. Kukushkina, D.A. Kirilenko, V.V. Shnitov, A.V. Shvidchenko, B. Senkovskiy, M.S. Shestakov, A.Ya. Vul', Rehybridization of carbon on facets of detonation diamond nanocrystals and forming hydrosols of individual particles, Carbon 122 (2017) 737-745, https://doi.org/10.1016/j.carbon.2017.07.013

[28] A.T. Dideykin, A.E. Aleksenskiy, D. Kirilenko, P. Brunkov, V. Goncharov, M. Baidakova, D. Sakseev, A.Ya. Vul', Monolayer graphene from graphite oxide, Diam. Relat. Mater. 20 (2011) 105-108, https://doi.org/10.1016/j.diamond.2010.10.007

[29] A.I. Kuklin, A.V. Rogachev, D.V. Soloviov, O.I. Ivankov, Y.S. Kovalev, P.K. Utrobin, S.A. Kutuzov, A.G. Soloviev, M.I. Rulev, V.I. Gordeliy, Neutronographic investigations of supramolecular structures on upgraded small-angle spectrometer YuMO, J. Phys.: Conf. Ser. 848 (2017) 012010, https://doi.org/10.1088/1742-6596/848/1/012010

[30] A.G. Soloviev, T.M. Solovjeva, O.I. Ivankov, D.V. Soloviov, A.V. Rogachev, A.I. Kuklin, SAS program for two-detector system: seamless curve from both detectors, J. Phys.: Conf. Ser. 848 (2017) 012020, https://doi.org/10.1088/1742-6596/848/1/012020

[31] C.E. Blanchet, A. Spilotros, F. Schwemmer, M.A. Graewert, A. Kikhney, C.M. Jeffries, D. Franke, D. Mark, R. Zengerle, F. Cipriani, S. Fiedler, M. Roessle, D.I. Svergun, Versatile sample environments and automation for biological solution X-ray scattering experiments at the P12 beamline (PETRA III, DESY). J. Appl. Cryst. 48 (2015) 431-443, https://doi.org/10.1107/S160057671500254X

[32] L.A. Feigin, D.I. Svergun, Structure analysis by small-angle X-ray and neutron scattering, Plenum Press: New York, 1987, 335 p.

[33] G. Beaucage, Approximations leading to a unified exponential/power-law approach to small-angle scattering, J. Appl. Cryst. 28 (1995) 717-728, https://doi.org/10.1107/S0021889895005292

[34] O.V. Tomchuk, D.S. Volkov, L.A. Bulavin, A.V. Rogachev, M.A. Proskurnin, M.V. Korobov, M.V. Avdeev, Structural characteristics of aqueous dispersions of detonation

nanodiamond and their aggregate fractions as revealed by small-angle neutron scattering, J. Phys. Chem. C 119 (1) (2015) 794−802, https://doi.org/10.1021/jp510151b

Figure captions

Fig. 1. (a) Size distribution of GO particles measured by light diffraction; inset shows schematic model of GO aqueous dispersion. (b) Size distribution of DND particles in aqueous dispersion measured by DLS; inset shows a scheme of colloidal aggregates of DND particles in aqueous dispersion.

Fig. 2. (a) Scattering spectrum of suspension of the graphene oxide (points); SAXS curve is scaled to SANS one. Solid line is model line for thin disk ($R > 500$ nm) with thickness 0.5 nm. (b) Dependence of neutron scattering intensity I from scattering vector q on DND aqueous dispersions at different concentrations (filled points). Inset: SANS curves normalized to concentration (empty points) are described by a unified exponential/power-law approach for fractal aggregates [33]. (c) Scattering curves on mixtures of DND and GO aqueous dispersions (filled points) obtained at different mass ratios of GO and DND designated as χ. Inset shows critical behavior of normalized SANS curves (empty points) due to remarkable changes in a scattering form-factor at high GO loading.

Fig. 3. TEM image of the composite obtained by mixing DND and GO aqueous dispersions.

Fig. 4. (a) On the basis of scattering data, schematic representation of structural organization of DND and GO aqueous dispersions. (b) The sensitivity of the TEM and SANS methods to the structure of thin graphene layers is separately shown. The presence of nanodiamonds on the surface of a graphene sheet increases both thickness and density from SANS viewpoint.

Fig. 5. Comparison of SANS curves on composite suspensions obtained by comparatively slight and intensive mixing of aqueous suspensions of GO and DND.

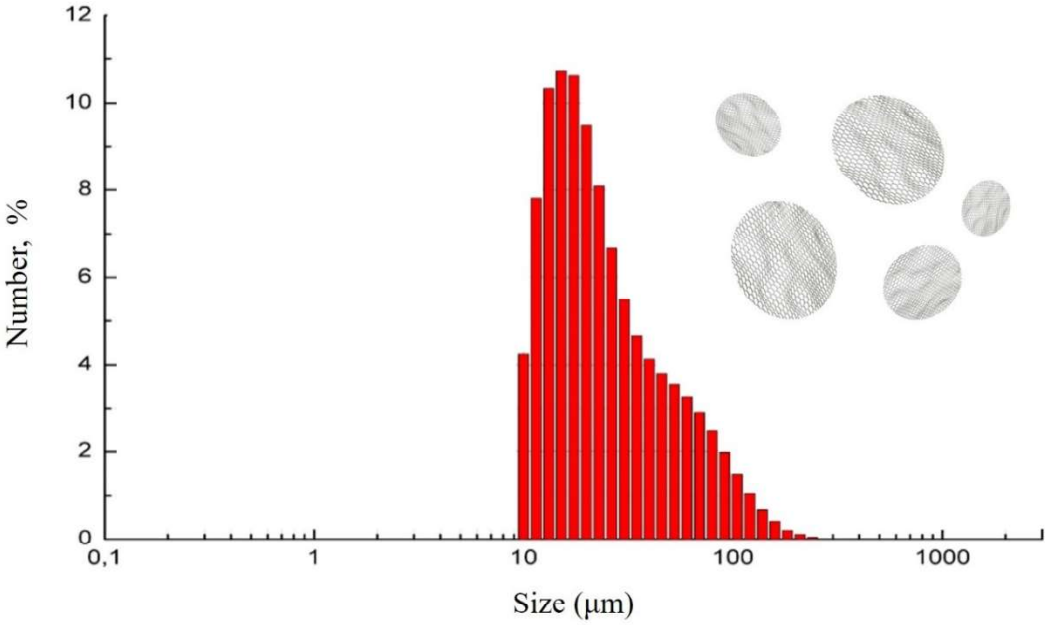
Number, %
12
10
8
6
4
2
0
0,1
1
10
100
1000
Size (μm)

Fig 1(a)

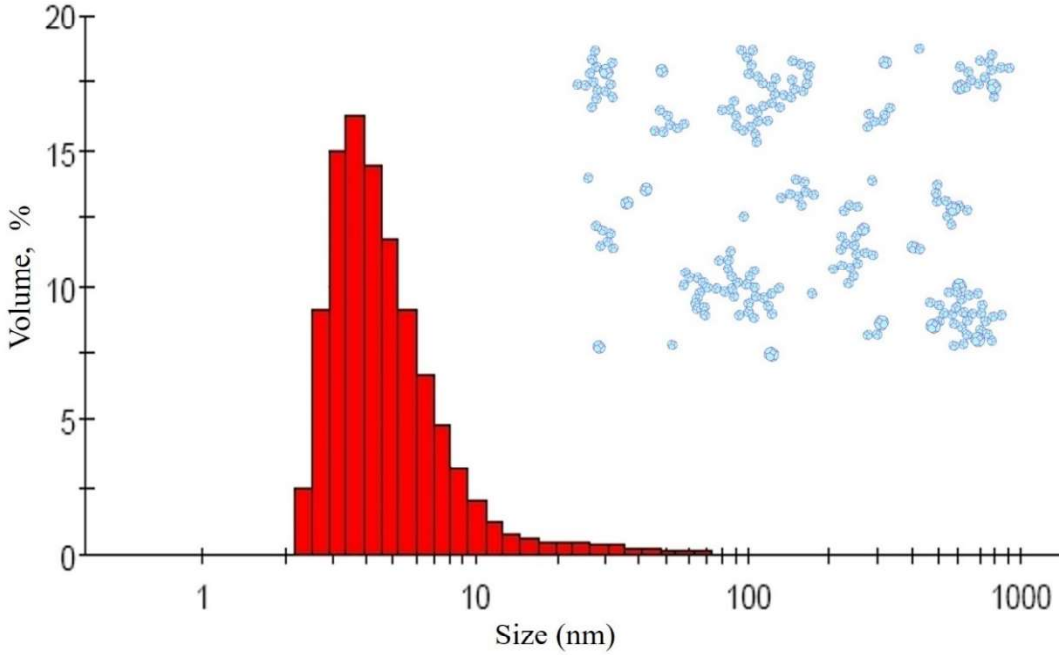
Volume, %
20
15
10
5
0
1
10
100
1000
Size (nm)

Fig 1(b)

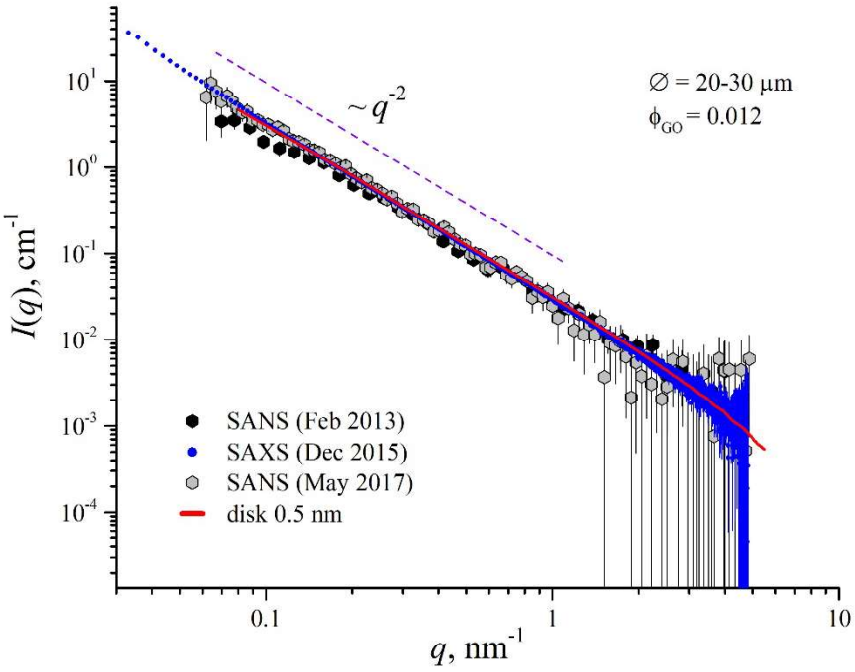
∅ = 20-30 μm
ϕGO = 0.012
~q-2
SANS (Feb 2013)
SAXS (Dec 2015)
SANS (May 2017)
disk 0.5 nm
I(q), cm-1
q, nm-1

Fig 2(a)

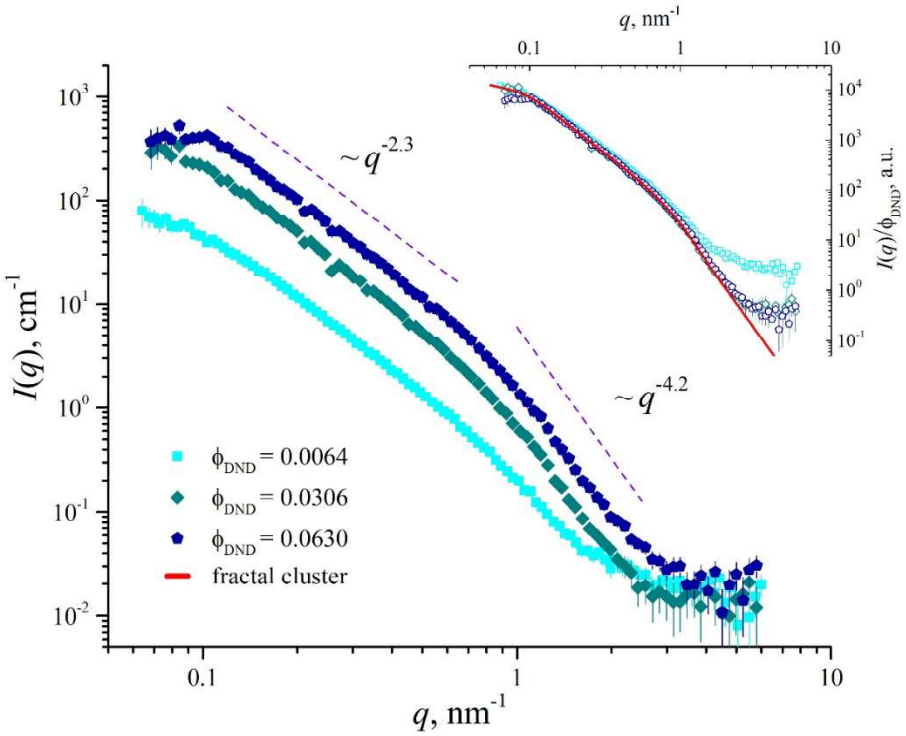
~q-2.3
~q-4.2
ϕDND = 0.0064
ϕDND = 0.0306
ϕDND = 0.0630
fractal cluster
I(q), cm-1
q, nm-1
I(q)/ϕDND, a.u.

Fig 2(b)

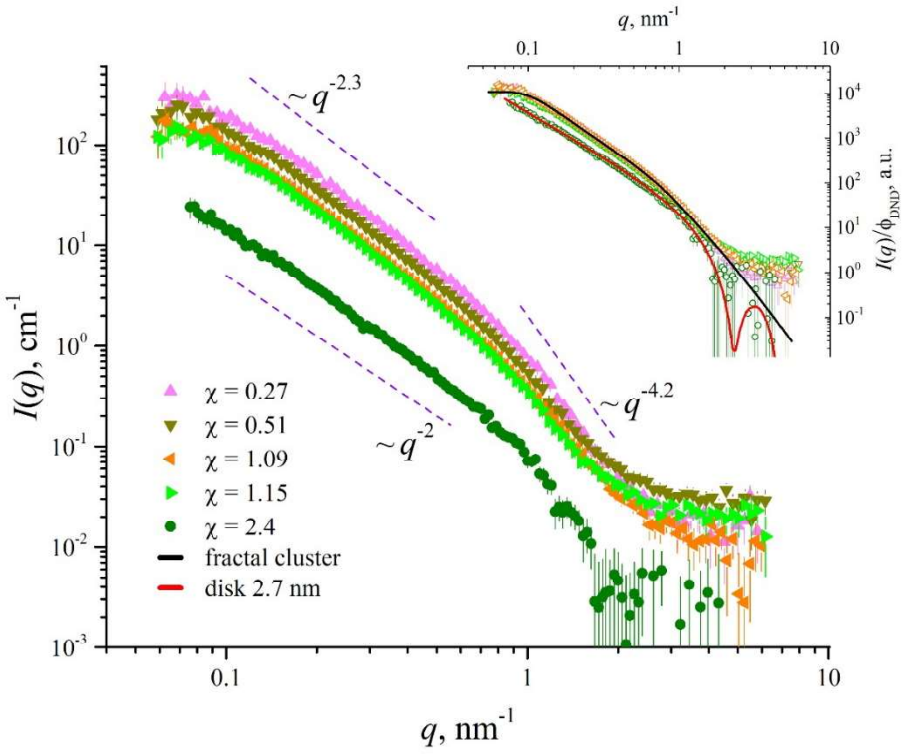
q, nm-1
0.1
1
10
~ q-2.3
~ q-4.2
~ q-2
χ = 0.27
χ = 0.51
χ = 1.09
χ = 1.15
χ = 2.4
fractal cluster
disk 2.7 nm
I(q), cm-1
I(q)/ϕDND, a.u.

Fig 2(c)

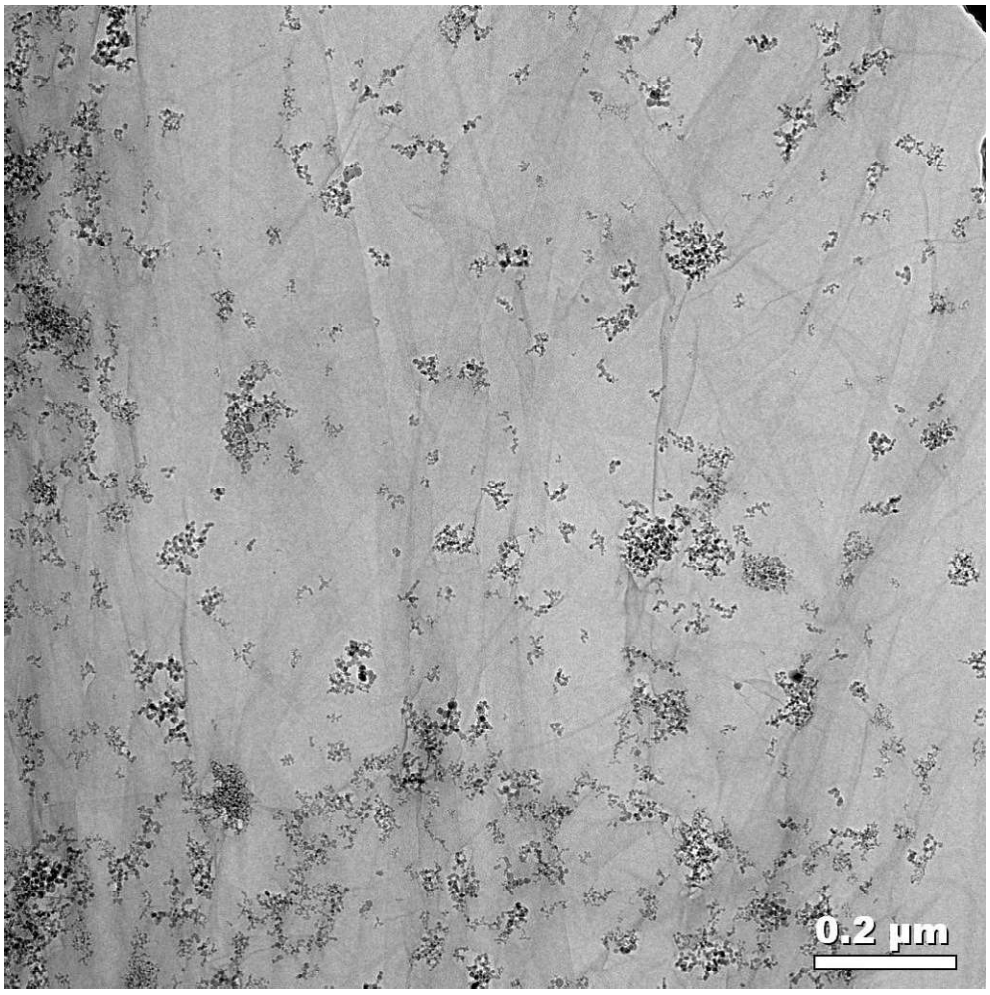
0.2 μm

Fig 3

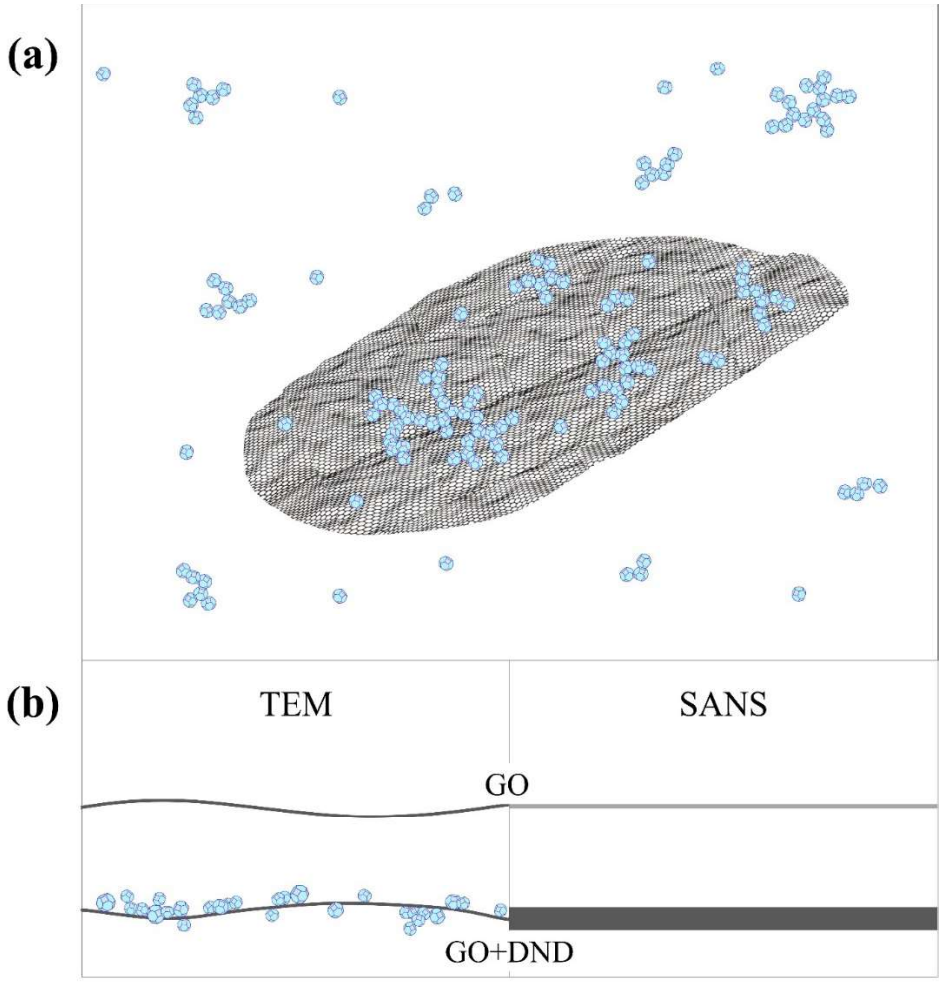
(a)
(b)
TEM
SANS
GO
GO+DND

Fig. 4

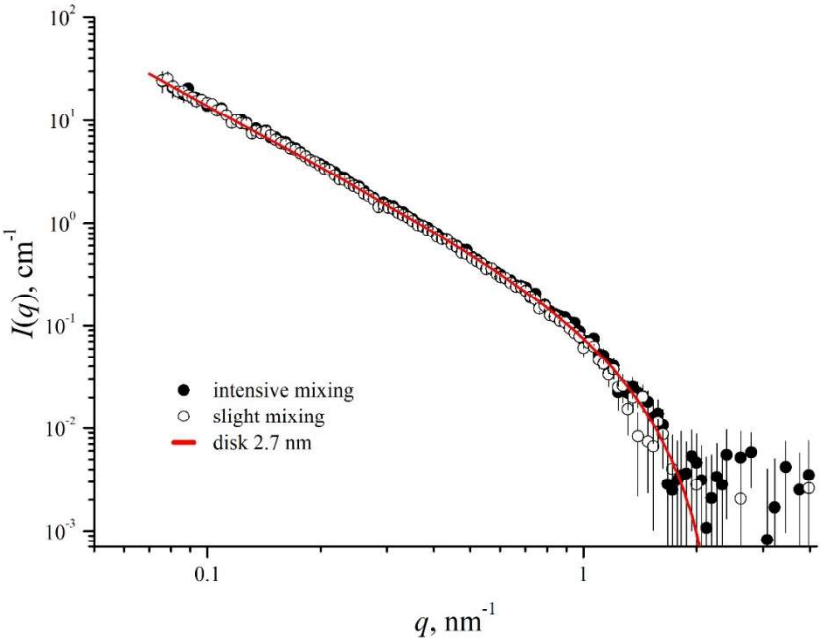
I(q), cm-1
q, nm-1
intensive mixing
slight mixing
disk 2.7 nm
0.1
1

Fig 5

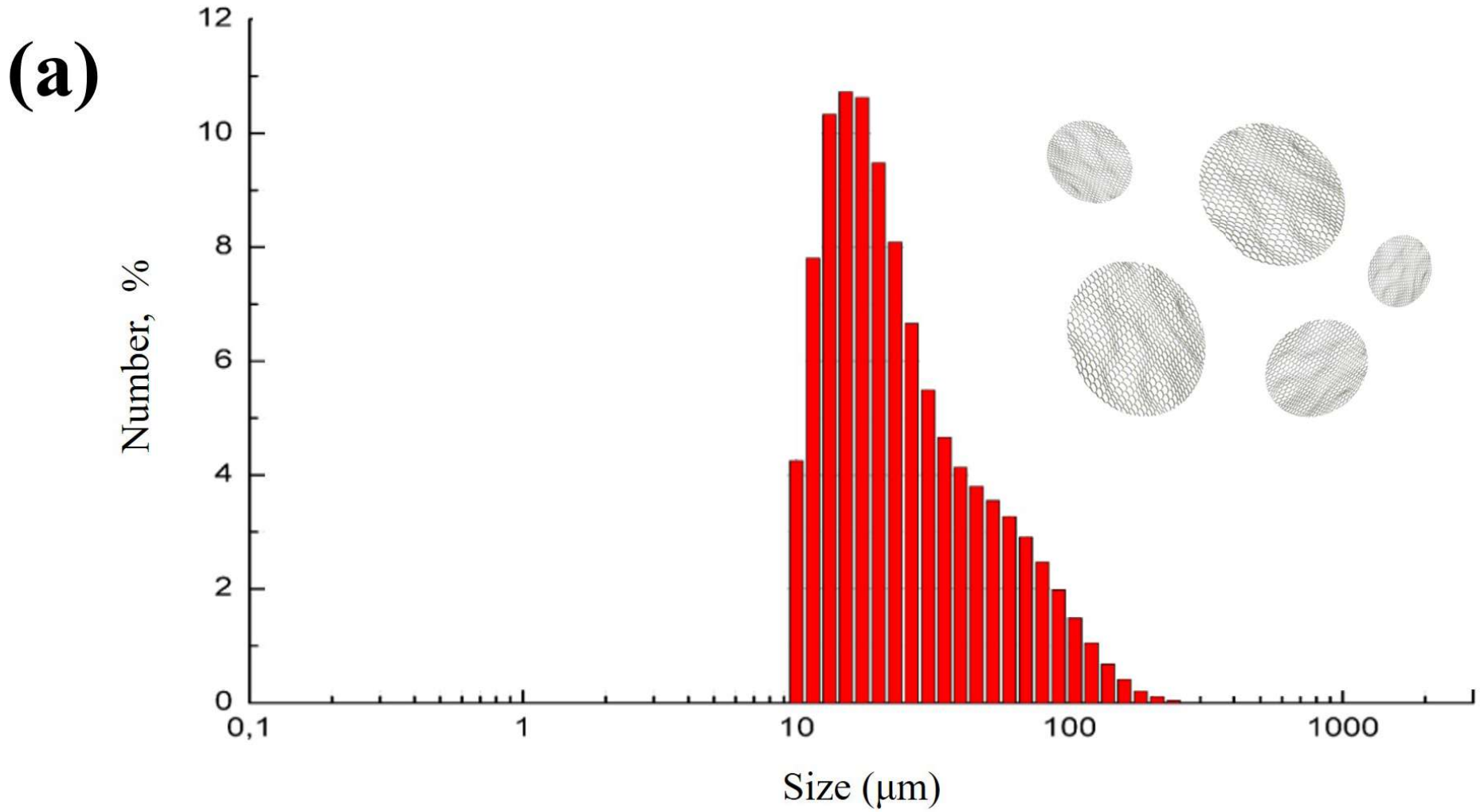
(a)
12
10
8
6
4
2
0
Number, %
0,1
1
10
100
1000
Size (μm)

(b)

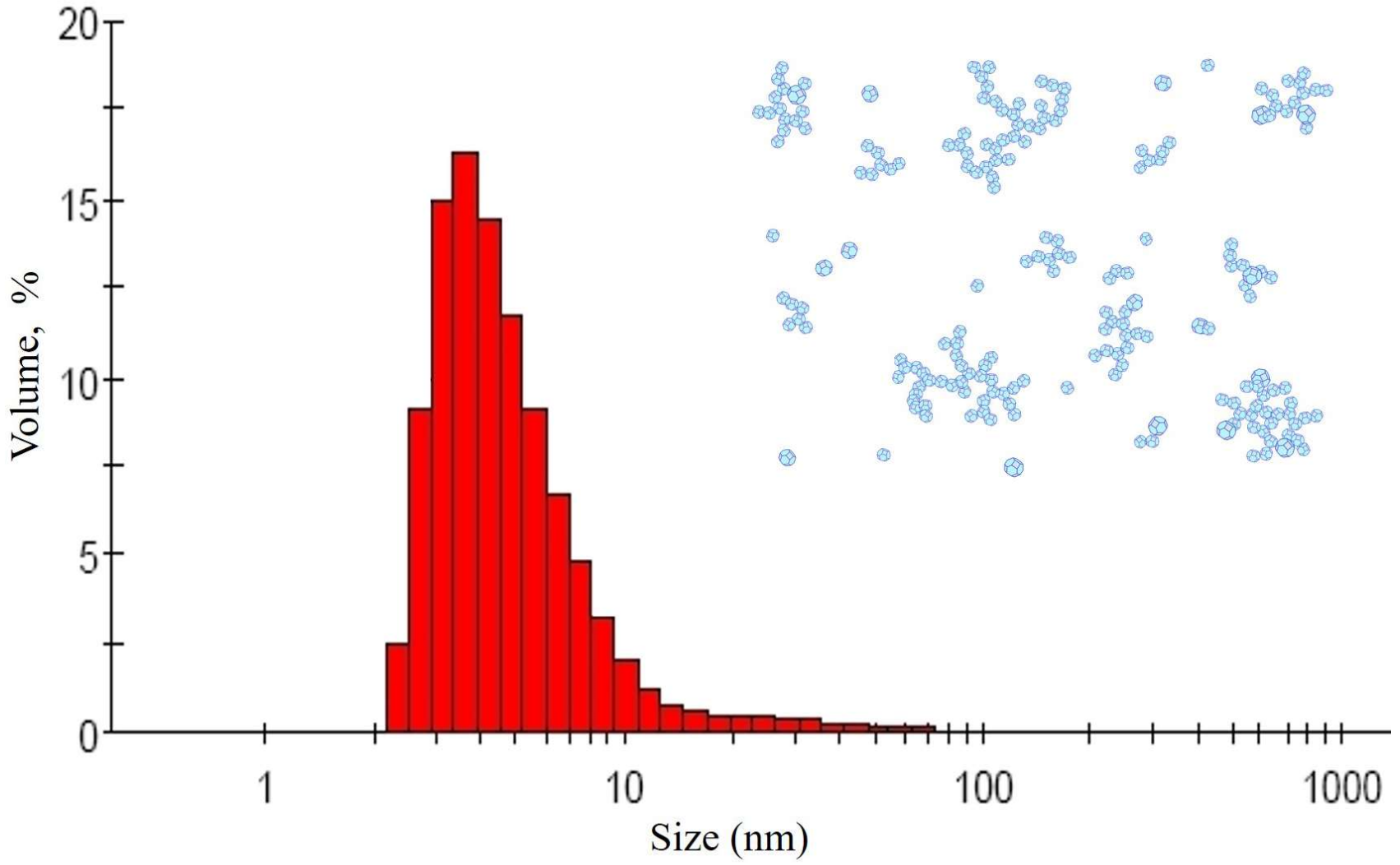

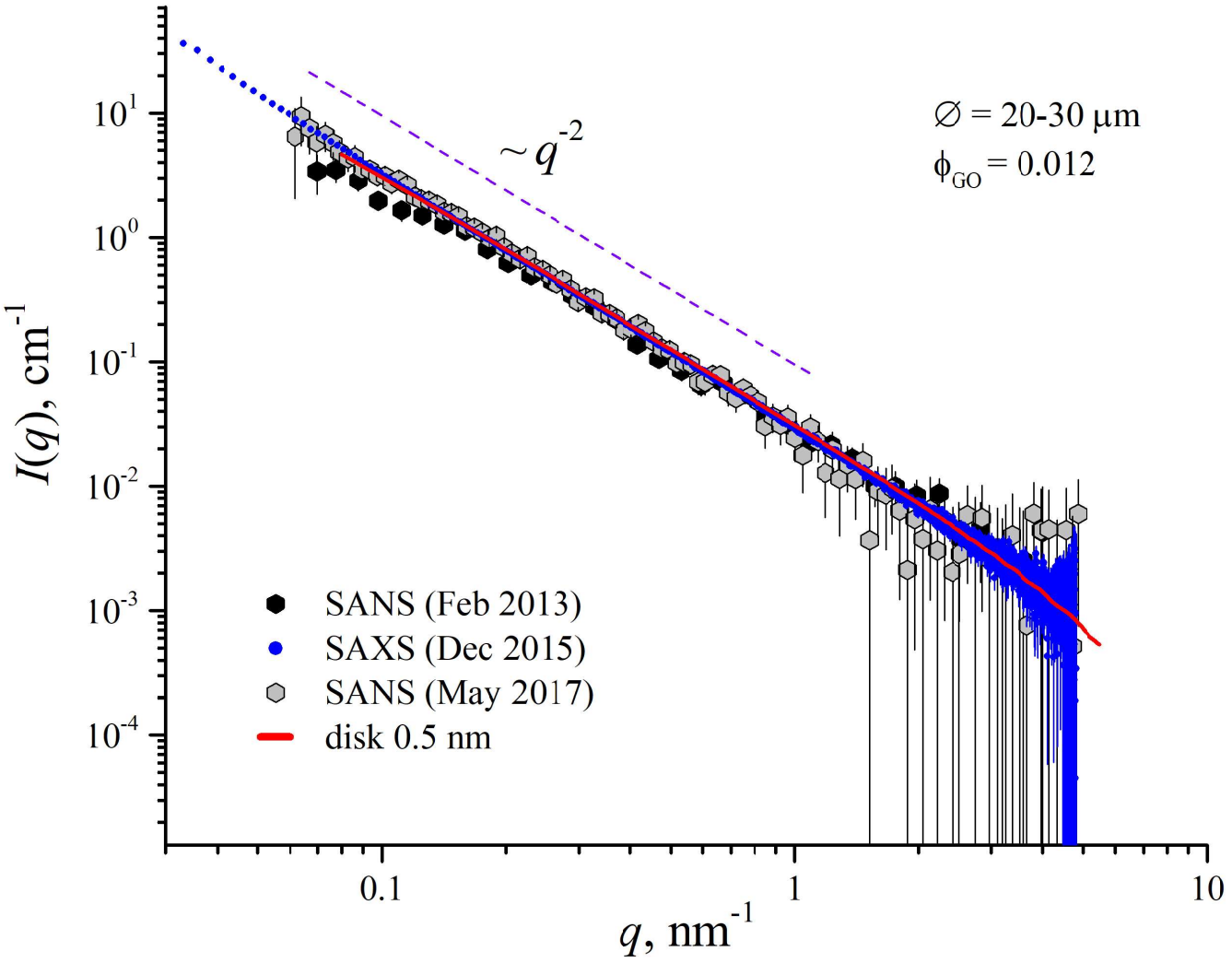
10^1
10^0
10^{-1}
10^{-2}
10^{-3}
10^{-4}
$I(q)$, cm^{-1}
$\sim q^{-2}$
∅ = 20-30 μm
ϕ_{GO} = 0.012
SANS (Feb 2013)
SAXS (Dec 2015)
SANS (May 2017)
disk 0.5 nm
0.1
1
10
q, nm^{-1}

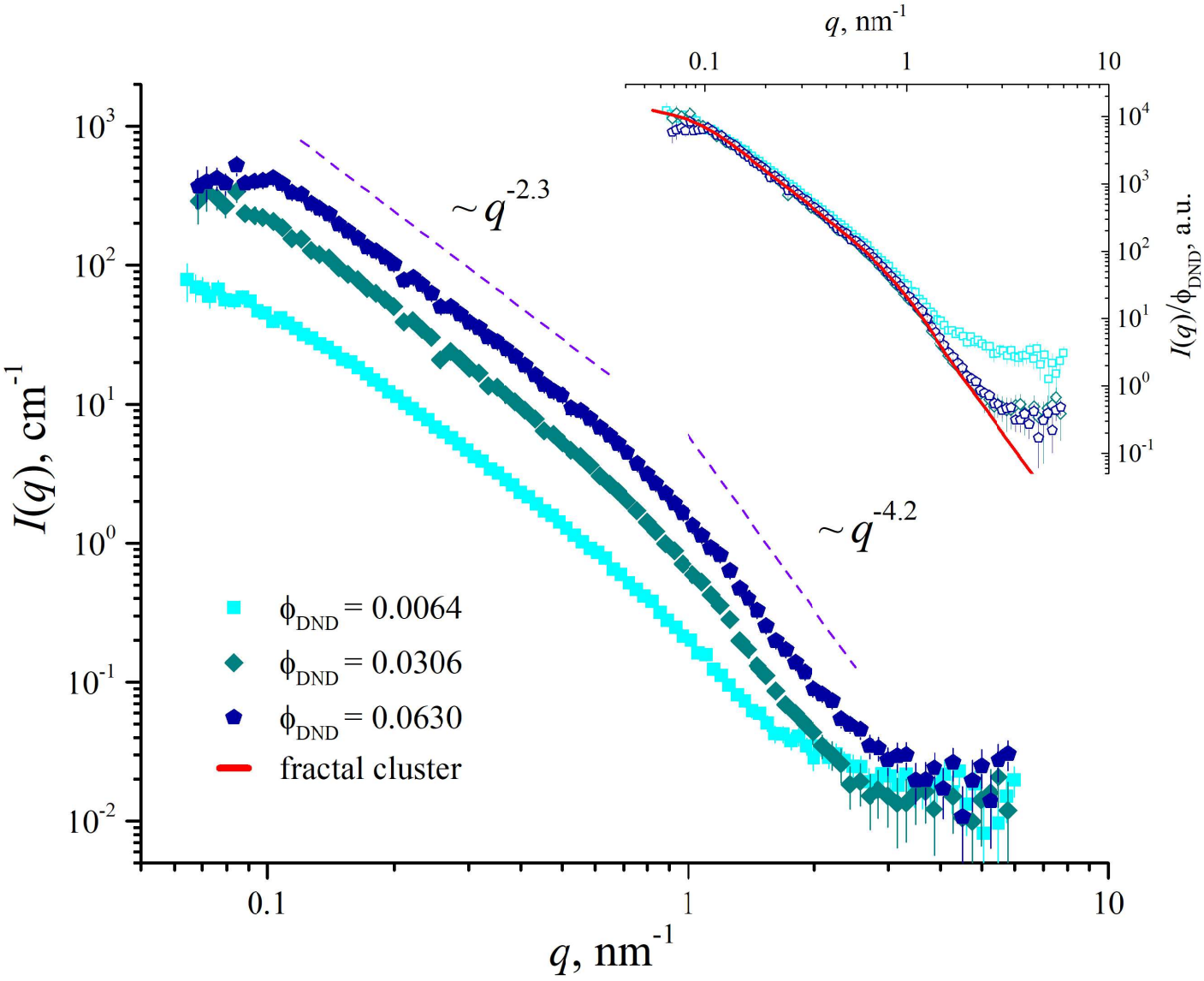
$I(q)$, cm^{-1}
q, nm^{-1}
0.1
1
10
10^{3}
10^{2}
10^{1}
10^{0}
10^{-1}
10^{-2}
$\sim q^{-2.3}$
$\sim q^{-4.2}$
ϕ_{DND} = 0.0064
ϕ_{DND} = 0.0306
ϕ_{DND} = 0.0630
fractal cluster
$I(q)/\phi_{DND}$, a.u.
10^{4}

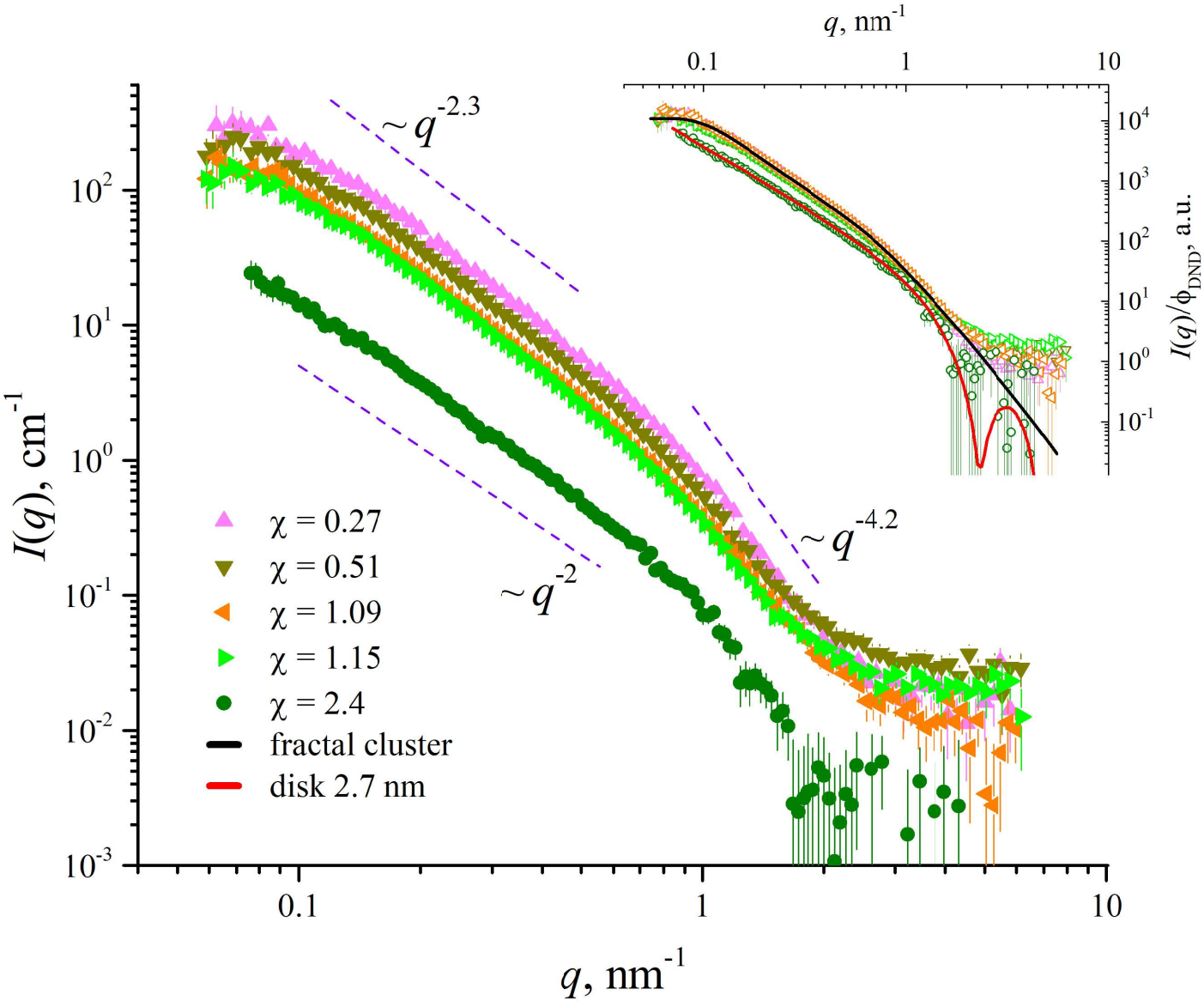
$I(q)$, cm^{-1}
q, nm^{-1}
$\sim q^{-2.3}$
$\sim q^{-4.2}$
$\sim q^{-2}$
χ = 0.27
χ = 0.51
χ = 1.09
χ = 1.15
χ = 2.4
fractal cluster
disk 2.7 nm
$I(q)/\phi_{DND}$, a.u.

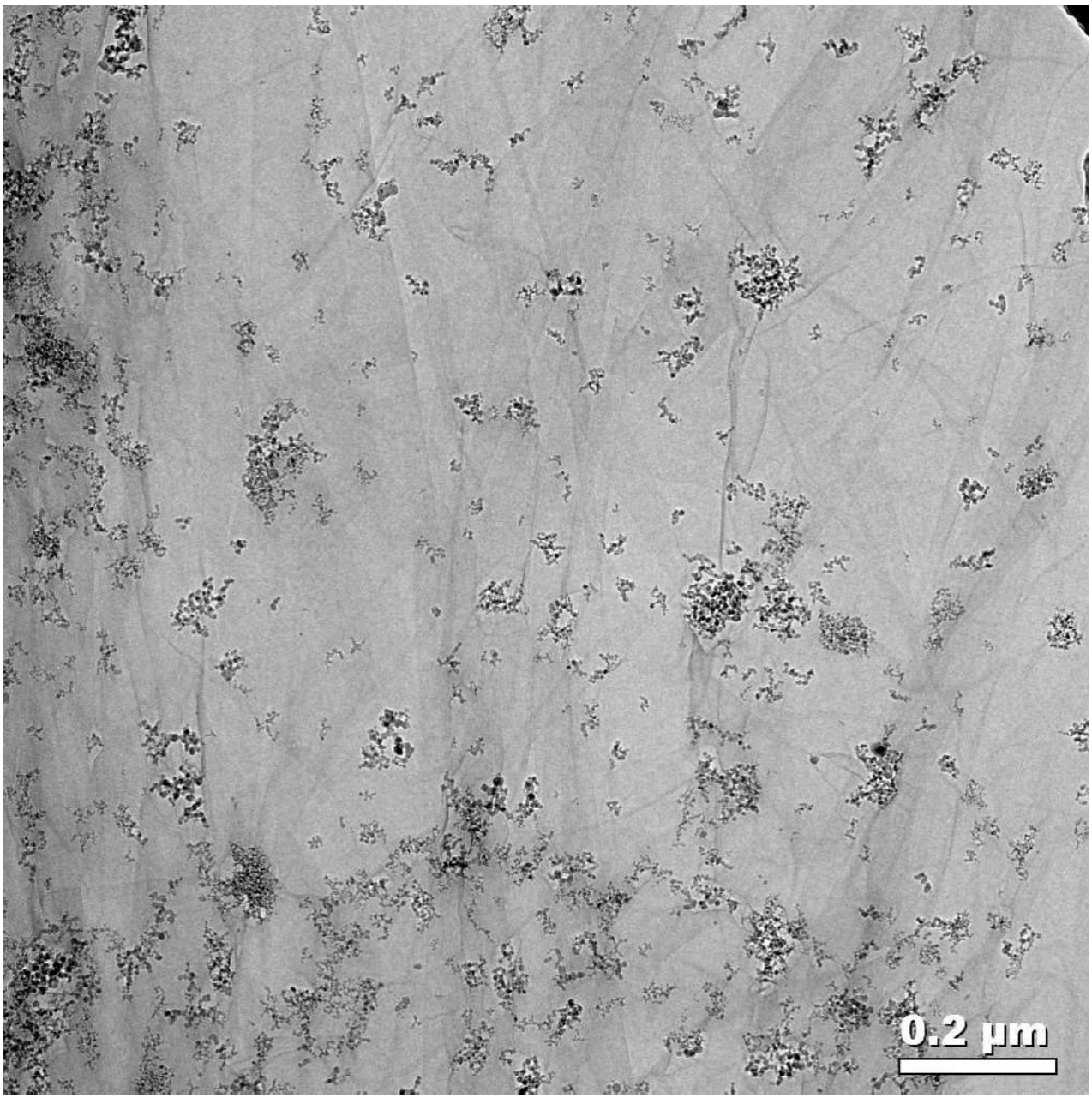
0.2 µm

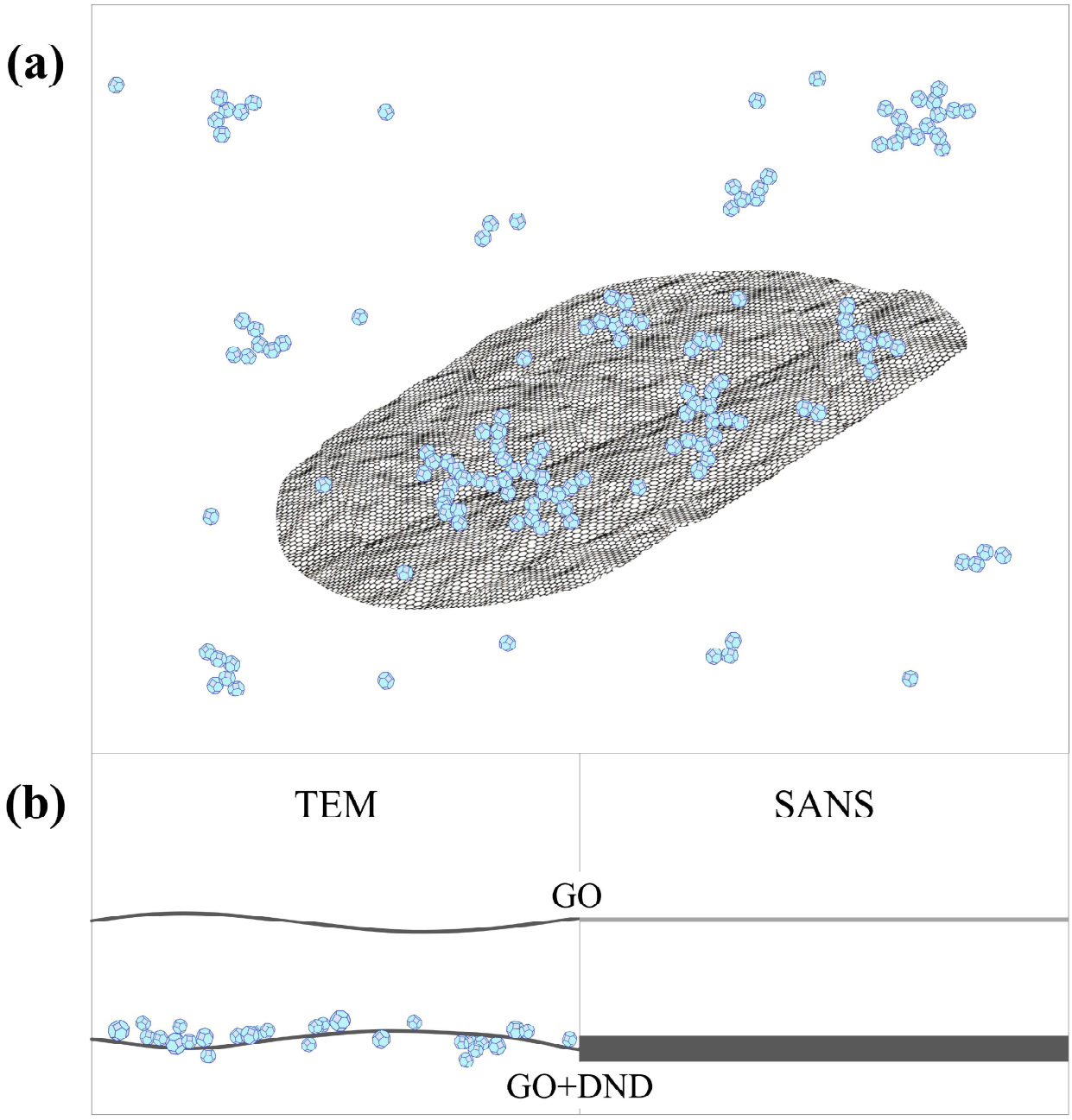
(a)
(b)
TEM
SANS
GO
GO+DND

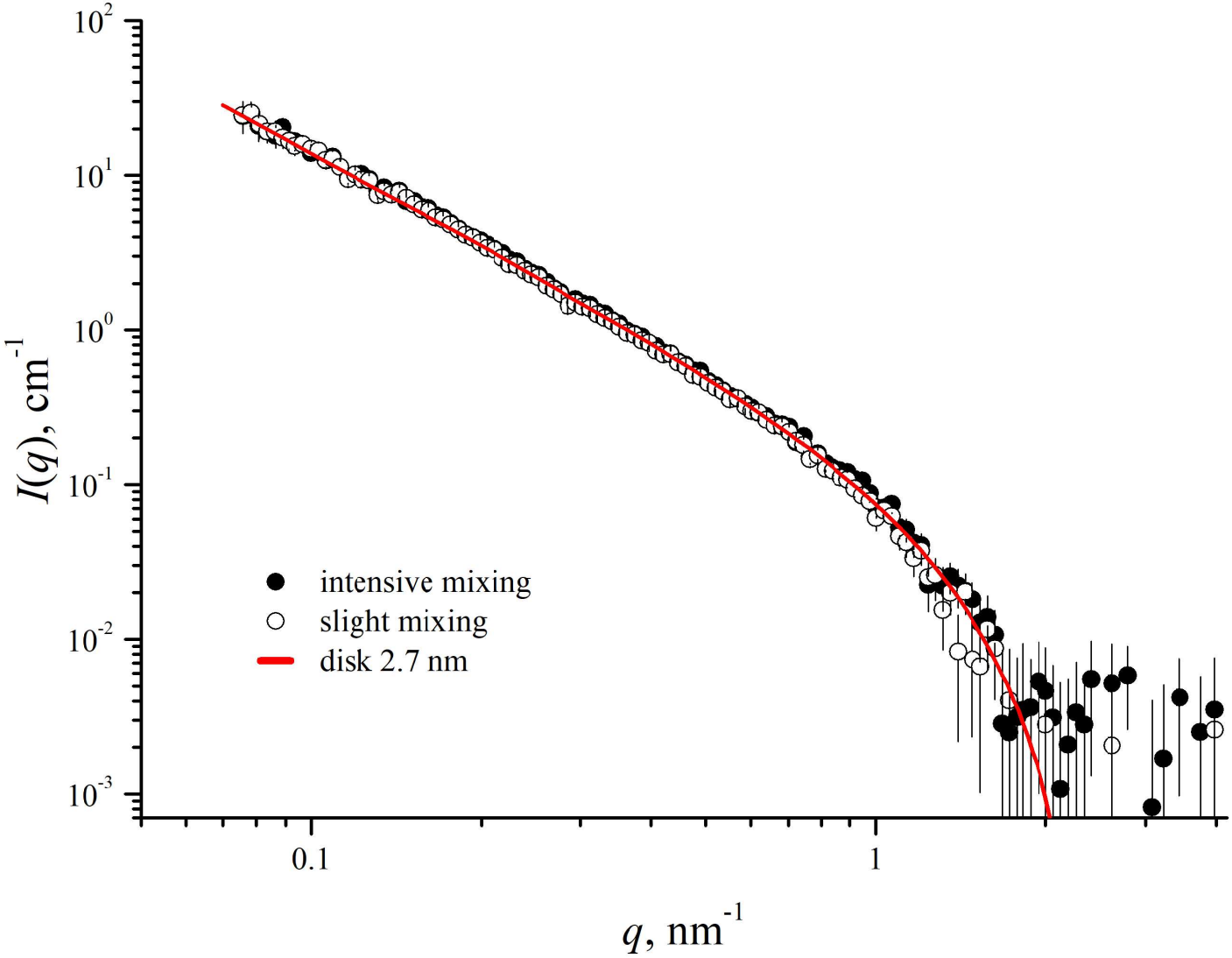
10^2
10^1
10^0
10^{-1}
10^{-2}
10^{-3}
$I(q)$, cm^{-1}
intensive mixing
slight mixing
disk 2.7 nm
0.1
1
q, nm^{-1}